IEEE Access
Multidisciplinary | Rapid Review | Open Access Journal

Received October 21, 2019, accepted October 30, 2019, date of publication November 4, 2019, date of current version November 14, 2019.

Digital Object Identifier 10.1109/ACCESS.2019.2951371

Compact Clock-Shaped Broadband Circularly Polarized Antenna Based on Characteristic Mode Analysis

MIN HAN, (Student Member, IEEE), AND WENBIN DOU, (Senior Member, IEEE)
State Key Laboratory of Millimeter Waves, Southeast University, Nanjing 210096, China

Corresponding author: Min Han (hanmin@seu.edu.cn)

This work was supported in part by the National Natural Science Foundation of China under Grant 61671146, and in part by the Fundamental Research Funds for the Central University under Grant 4004009104.

ABSTRACT This paper presents the design process of a clock-shaped broadband circular polarized (CP) antenna based on Characteristic Mode Analysis (CMA). It is composed of a circular ring, two microstrip lines approximately perpendicular to each other, and 50-Ω improved coplanar waveguide (CPW). The two microstrip lines are introduced in the X and Y directions, respectively, to break the symmetry for CP operation. Different from the conventional method in which the operation is verified by the simulated surface current distribution, CMA provides physical insight into different modes of the antenna and reveals the mechanism of radiating CP wave. Mode currents and characteristic fields of the selected modes are studied for AR bandwidth enhancement. An improved double-sided printed CPW is introduced to excite the desired modes and achieve wideband impedance matching. To validate the proposed concept, a prototype with a compact size of $0.29\lambda_L \times 0.29\lambda_L \times 0.013\lambda_L$ (λ_L corresponding to the maximum operation frequency) is fabricated and measured. The measured -10 dB impedance bandwidth and 3 dB AR bandwidth are 84.6% from 2.38 GHz to 5.8 GHz and 43.4% from 2.4 GHz to 3.73 GHz, respectively. The overlapping operating bandwidth can cover the ISM band, the TD-LTE band, and the WiMAX band. Besides, the proposed antenna has a stable radiation pattern over the operating band.

INDEX TERMS Broadband antennas, characteristic mode analysis (CMA), circular polarization (CP), co-planar waveguide (CPW).

I. INTRODUCTION

Circularly polarized (CP) antennas have attracted extensive attention in high-capacity wireless communications and high-resolution radar systems because of combatting multi-path interferences or fading, reducing the 'Faraday rotation' effect, and overcoming polarization mismatch between a transmitter and a receiver. Nevertheless, the bandwidth is still a challenge in practical design.

CP radiation can be regarded as the combination of two orthogonal linearly polarized (LP) radiations with equal amplitude and 90° phase difference. Asymmetric radiators are widely used to generate the desired CP radiations, such as asymmetric patches with L-shaped slots [1], asymmetric defective ground [2], a square patch with two connected slots to realize defective ground [3], the stacked patch with cutting symmetrical angles [4]. Utilizing perturbations in the forms of feed lines [5]–[7], slot structures [8]–[10] and array configurations [11], [12] have also been proposed. Most of these designs are achieved by full-wave simulation and optimization based on engineering experience and intuition with little physical insight.

All of the antenna properties can be obtained by full-wave simulation, such as the radiation patterns, input impedance, and radiation efficiency. The final simulated physical characteristics depend on whether the resonant properties of the antenna itself are excited by the external source. Improper feeding results in the current distribution not reflecting the natural resonance characteristics of the antenna. The natural resonant behavior of antenna is conducive to further optimization and design of the feed structures. Characteristic Mode Analysis (CMA) provides a source-free method to

The associate editor coordinating the review of this manuscript and approving it for publication was Giorgio Montisci.

This work is licensed under a Creative Commons Attribution 4.0 License. For more information, see http://creativecommons.org/licenses/by/4.0/

analyze the resonant behavior of antenna structure. The CMA was first proposed by Garbacz [13], and improved by Harrington and Mautz in the 1970s [14]. The CMA allows obtaining the resonant frequencies of fundamental modes as well as those higher-order modes in the absence of excitation. It also describes the resonance property of each mode on the electromagnetic structure and the radiation behavior in the far-field zone. Different characteristic current modes are orthogonal to each other on the surface of the conductor, and their corresponding characteristic fields are orthogonal at infinity [15]. These valuable modal analysis results provide guidance for optimization to achieve desired radiation performance at a specific frequency [16], [17]. In [18], CMA was first used to analyze metasurface, and multiple modes were excited simultaneously to achieve broadband. Soon after, CMA was successfully used to solve the coupling problem of metasurface multiport antennas and improved the problem of pattern distortion [19]. With the help of CMA, the resonant frequencies of different modes for metasurface were independently controlled for dual-band 5G applications [20]. In [21], S-band and K-band antennas with a common aperture were designed based on the multi-mode of metasurface by CMA. In [22], CMA successfully revealed that surface wave, leakage wave, and mixing of multiple resonance modes together contribute to the broadband of the SIW-fed end-fire metasurface antenna. CMA was also used to design stacked antenna [23] and RFID Tag [24].

This paper proposes a novel CP antenna with an integrated feed structure designed by CMA. A circular ring is first analyzed based on the theory of characteristic mode, and a pair of degenerate modes with orthogonal polarization are selected for further optimization. Two microstrip lines are proposed to reconfigure the selected modes with a certain Characteristic Angle (CA) difference. Furthermore, anther two modes are introduced for wideband CP operation. Then the feeding structure placement is determined to excite the selected modes based on CMA. Finally, the full-wave simulation of the proposed antenna is carried out for final optimization. All simulation results are obtained by Computer Simulation Technology (CST) and FEKO.

II. CP GENERATION FOR CLOCK-SHAPED ANTENA

A. CHARACTERISTIC MODE THEORY

The characteristic modes (CMs) are a complete set of orthogonal modes for expanding any induced currents and far-fields due to a specific external source. In other words, the induced currents on the PEC body can be written as a superposition of the characteristic currents.

$$\mathrm{J} = \sum\nolimits_n c_\mathrm{n} \cdot \mathrm{J_n} \tag{1}$$

where $\mathrm{J_n}$ is the characteristic current of mode n, c_n is the complex modal weighting coefficients (MWC) for each mode, measures the contribution of each mode in the total electromagnetic response to a given source, and can be expressed as [15]:

$$|c_\mathrm{n}| = 1/|1 + j\lambda_\mathrm{n}| \cdot |\int \mathrm{J_n} \cdot \mathrm{E_i}\, \mathrm{dS}| = \mathrm{MS} \cdot |v_\mathrm{n}| \tag{2}$$

Here, v_n is the modal excitation coefficient (MEC), which measures the contribution of each mode in the total electromagnetic response to a given source.

$$v_\mathrm{n} = \int \mathrm{J_n} \cdot \mathrm{E_i dS} \tag{3}$$

MS is the modal signification (MS), which is the normalized amplitude of the characteristic current. If the MS of a CM is greater than $1/\sqrt{2}$, it is a significant mode and vice versa.

$$\mathrm{MS} = 1/|1 + \mathrm{j}\lambda_\mathrm{n}| \tag{4}$$

Equation (2) shows that to excite the desired mode, a large MS and a large MEC are necessary. The MEC is strongly correlated with the position, magnitude, phase, and polarization of the external source. The optimal excitation position can be determined by the MEC.

Another critical physical parameter is Characteristic Angle (CA), which is defined as follows:

$$\mathrm{CA} = 180^\circ - \tan^{-1}(\lambda_\mathrm{n}) \tag{5}$$

CA is the phase angle lag between the real characteristic current and its associated characteristic field, evaluating the corresponding behavior of each CM. Notably, whether two orthogonal modes achieve CP radiation with only one feed can be estimated by the CA information.

To generate CP radiation, two orthogonal modes should be excited simultaneously with 90° CA difference. Thus, the requirements for these two modes are:

1. The mode current distributions are orthogonal to each other,
2. The MSs are the same: $\mathrm{MS}_1 = \mathrm{MS}_2$,
3. The CA difference is 90°: $|\mathrm{CA}_1 - \mathrm{CA}_2| = 90^\circ$.
4. The directivities are the same at the angle of interest.

B. EXISTING MODE OF THE RING

The resonance property of each mode on the electromagnetic structure and the radiation behavior in the far-field can be obtained by CMA in the absence of excitation.

To demonstrate the design principle, the CMA is first carried out form a ring, as a guide to the more complicated structure. To note that the substrate (FR4 with $\varepsilon_\mathrm{r} = 4.4$ and thickness of 1.6mm) is assumed to be loss-free and infinite. The ring patch is designed near 3 GHz with a large radius of 13 mm and a small radius of 12.5 mm, as shown in Fig. 1.

The first six characteristic modes are calculated in terms of MS and CA, as shown in Fig. 2. Their corresponding mode currents (J1-J6) and characteristic fields at 2.7 GHz are shown in Fig. 3. The other modes are ignored due to the small MS. Modes 1 and 2 is a pair of degenerated modes, as well as Modes 4 and 5. Modes 1 and 2 resonate at 2.7 GHz. Modes 4 and 5 resonate at 5 GHz. At 4.4 GHz, the MSs

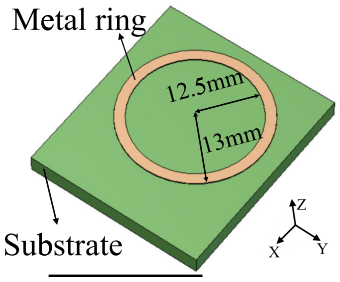

FIGURE 1. The geometry of the ring.

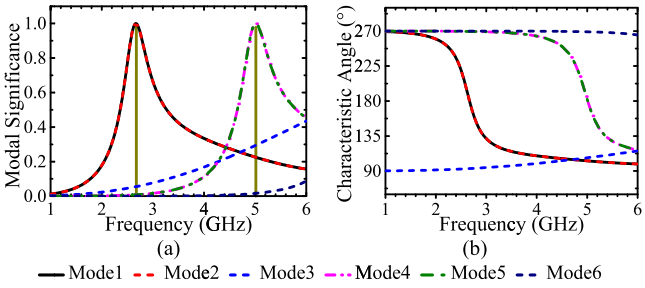

FIGURE 2. (a) Modal significance and (b) Characteristic angle for the first six modes of the ring.

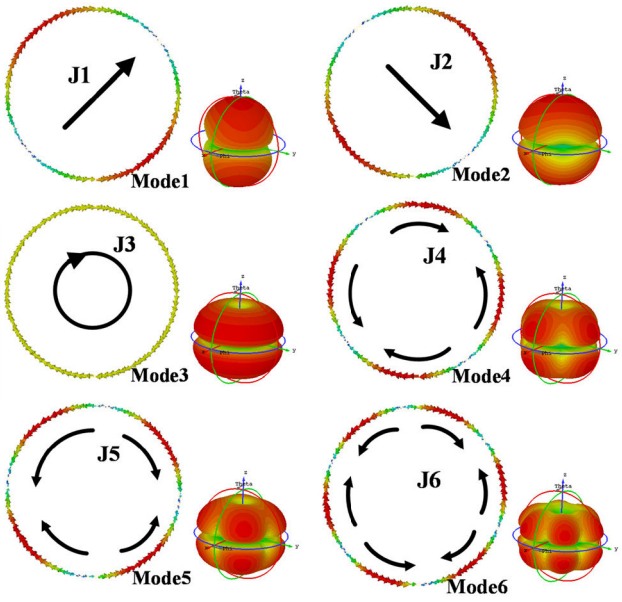

FIGURE 3. Mode current and characteristic field for first six modes of the ring at 2.7 GHz.

of Modes 1 and 2 are equal to the MSs of Modes 4 and 5. As shown in Fig. 3, only J1 and J2 radiate in the ±Z direction resulting from symmetric distribution on the XOY plane. Whereas J3-J6 are rotationally symmetric to the Z axis, leading to a null gain in ±Z direction in the far-field region. Around 2.7 GHz, Modes 1 and 2 are the operating modes with perpendicular mode currents and the similar characteristic field. However, the CA difference between the two modes is 0° meaning no contribution to the CP realization as well as J4 and J5.

C. EXISTING MODE OF THE PROTO A

To realize CP, the symmetrical ring structure needs to be disturbed to produce the desired characteristic modes with certain CA difference. As shown in Fig. 4, two microstrip lines are introduced in the X and Y direction, respectively. The Y one is directly added to the ring, and the X one is connected to the ring by a metal patch (named M connector) on the other side of the substrate, thereby avoiding the overlap. The new electrical structure is named Proto A. Fig. 5 shows the first six modes over 1 GHz–6 GHz.

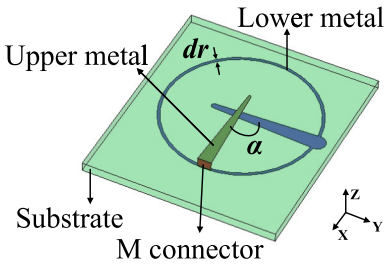

FIGURE 4. The geometry of the Proto A.

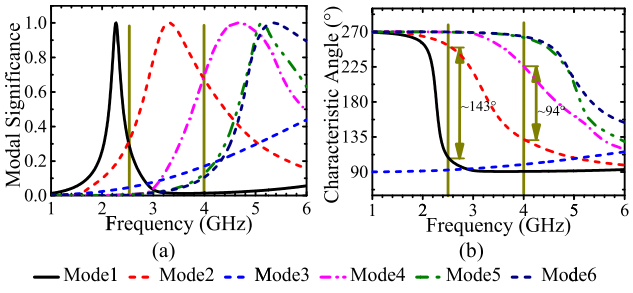

FIGURE 5. (a) Modal significance and (b) Characteristic angle for the first six modes of the Proto A.

At 2.5 GHz, only Modes 1 and 2 can be easily excited as the equivalent considerable MS. These two mode currents (J1 and J2) and characteristic fields are shown in Fig. 6. Both J1 and J2 are symmetrically distributed, and their equivalent currents are perpendicular to each other. The perpendicular mode currents (J1 and J2) and the 143° CA difference make Mode 1 and Mode 2 have the potential to generate CP radiation.

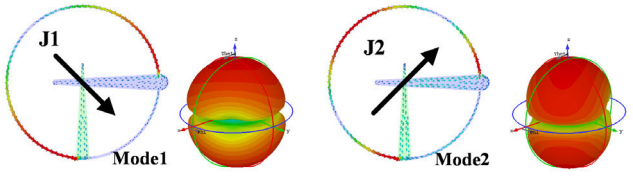

FIGURE 6. Mode current and Characteristic field for Mode 1 and Mode 2 of the Proto A at 2.5 GHz.

As the frequency increases, more modes with relatively large MS are involved. When the frequency rises to 4 GHz,

Modes 2 and 4 are the operating modes with the same MSs of 0.7. The corresponding mode currents and characteristic fields are shown in Fig. 7. Clearly, J2 and J4 are perpendicular to each other. Besides, a 90° CA difference between Modes 2 and Mode 4 is observed at 4 GHz.

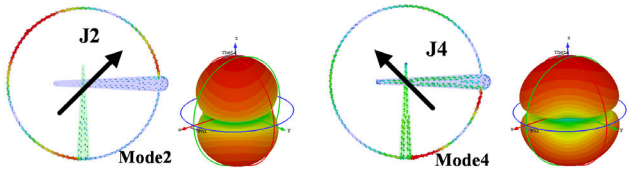

FIGURE 7. Mode current and Characteristic field for Mode 2 and Mode 4 of the Proto A at 4 GHz.

As shown in Fig. 5, in the band of 2.3 GHz–3.2 GHz, Modes 1 and 2 are operating modes with a CA difference between 78° and 144°. When the frequency increases to 3.2 GHz, the MS of Mode 1 decreases to zero and the MS of Mode 4 rises. From 3.2 GHz to 4.5 GHz, the CA difference between Mode 2 and 4 maintains between 70° and 94°. In other words, Proto A features CP potential over 2.3 GHz–4.5 GHz. When the frequency rises to 4.5 GHz, more modes are involved, and the CP performance is deteriorated.

To understand how to affect the characteristic mode of Proto A, the key parameters are studied. Simulation results show that the CA difference of the operating modes is correlated with the angle of two microstrip lines (α) and the ring width (dr). Fig. 8 shows the variation of CA difference between two operating modes versus frequency with different α and dr. There is a minimum point on the CA difference curve near 3 GHz because the operating modes of Proto A switch from Modes 1 and 2 to Modes 2 and 4. Fig. 8 shows that when dr is 0.5mm or 2mm, as α increases from 80° to 120°, the CA difference curve shifts downward and rightward before reaching the minimum value. After reaching the minimum value, the CA difference curve shifts downward and leftward. Considering the bandwidth and the potential to radiate CP waves, the optimal values of α and $dr$are 110° and 0.5mm, respectively. Finally, the CA difference ranges of 73°–137° and 57°–71° are achieved for Modes 1 and 2 at

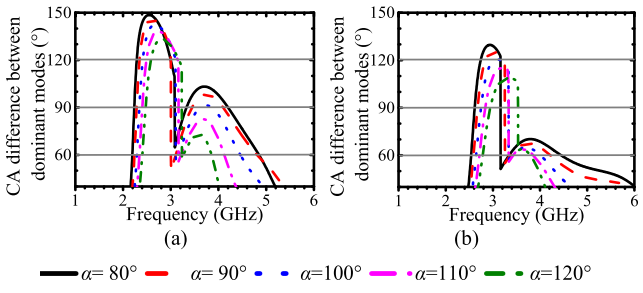

FIGURE 8. CA difference between operating modes versus frequency (a) when dr = 0.5mm, (b) when dr = 2mm.

2.38 GHz–3.16 GHz and Modes 2 and 4 at 3.1 GHz–4 GHz, respectively.

The MS and CA characteristics of the final Proto A are shown in Fig. 9, which indicates that the final Proto A has the potential to radiate CP waves in the band of the 2.38 GHz–4 GHz band.

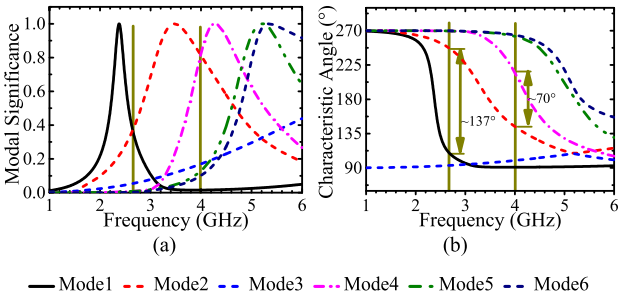

FIGURE 9. (a) Modal significance and (b) Characteristic angle for the first six modes of the final Proto A.

D. FEED STRUCTURE SETTING

Due to the source-independent solution of CMA, designing specific feeding structures is allowed to lag behind the shaping of the antenna geometry. A well-designed feed structure is needed to excite the selected CMs and suppress unwanted modes. Ideally, CP performance will appear when these operating modes are properly excited and combined. To excite operating modes with the same magnitude, the excitation should be set at the minimum difference between operating mode currents [25]. The MS crossover frequency of Modes 1 and 2 is 2.6 GHz, and the current difference distribution between the two is plotted in Fig. 10(a). The MS crossover frequency of Modes 2 and 4 is 4 GHz, and the current difference distribution between the two is plotted in Fig. 10(b). The M connector is an appropriate position for excitation because, in both cases, the current difference distribution of the operating modes is tiny.

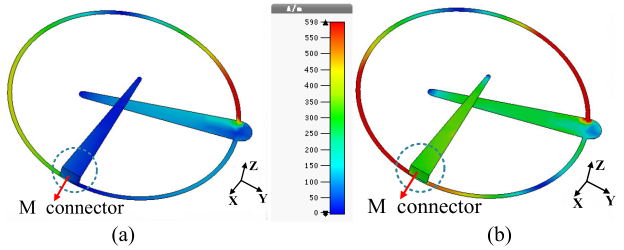

FIGURE 10. Current differ ence distribution (a) between J1 and J2 at 2.6 GHz, (b) between J2 and J4 at 4 GHz.

An improved double-sided printed CPW is selected as feed structure with the middle conductor and the ground plane connecting the upper metal strip and the lower ring of Proto A, respectively. The proposed antenna is shown in Fig. 11, and its first six characteristic modes are shown in terms of CM and MS in Fig. 12. Mode currents and characteristic fields are shown in Fig. 13. At 2.7 GHz–3.15 GHz, the operating modes of the proposed

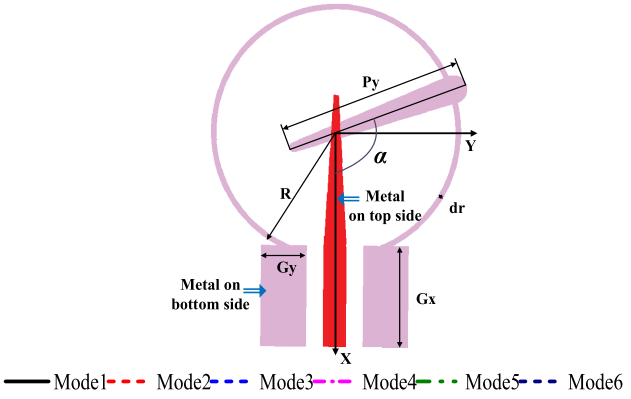

FIGURE 11. The geometry of the proposed antenna.

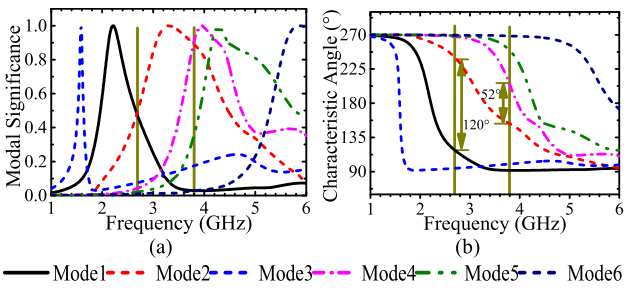

FIGURE 12. (a) Modal significance and (b) Characteristic angle for the first six modes of the proposed antenna.

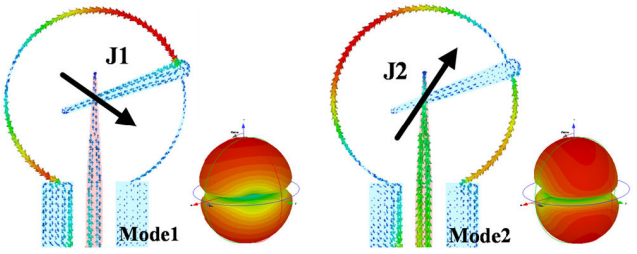

FIGURE 13. Mode current and Characteristic field for Mode 1 and Mode 2 of the proposed antenna at 2.65 GHz.

antenna are Modes 1 and 2, with mutually perpendicular mode currents, similar characteristic fields, and a CA differences of 96°–122°. At 3.15 GHz–3.78 GHz, Modes 2 and 4 play leading roles featuring perpendicular mode currents, similar characteristic fields, and a CA differences of 53°–67°. In other words, it is possible to achieve the CP condition over 2.7 GHz–3.78 GHz.

III. THE PROPOSED ANTENNA CHARACTERISTICS

The initial values of antenna parameters are determined by CMA in Section II. In order to improve antenna performance, the parameter α and dr are optimized by full-wave simulation.

The introduced microstrip lines alter the mode currents and produce orthogonal characteristic fields to generate a CP radiation, and therefore α has a significant influence on both of the impedance and AR bandwidth. Fig. 15 shows the variation of impedance and AR bandwidths with α increasing

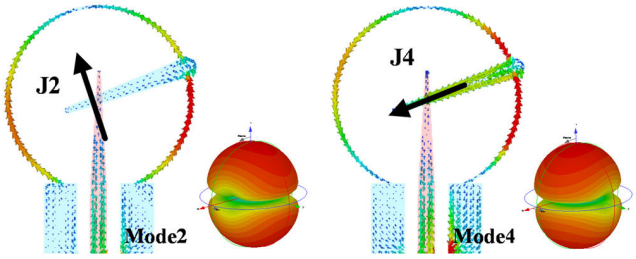

FIGURE 14. Mode current and Characteristic field for Mode 2 and Mode 4 of the proposed antenna at 3.78 GHz.

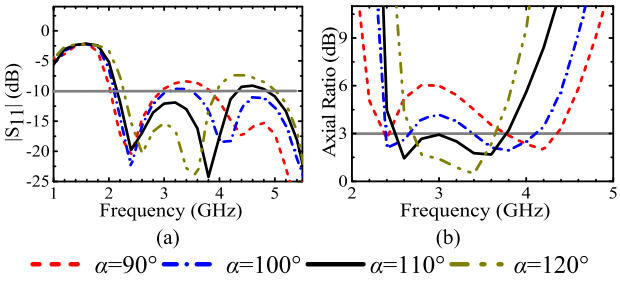

FIGURE 15. (a) Simulated $|S_{11}|$, and (b) AR of the proposed antenna with different α.

from 90° to 120°. As α increases, the first response frequency increases slightly, but the second response frequency decreases significantly with intensifying resonance. When α exceeds 100°, the $|S_{11}|$ between the first two resonance frequencies is less than −10 dB, and it continues to decline with the increase of α. As α increases, the first CP mode shifts to higher frequency, and the second CP mode shifts to lower frequency. The optimal value of α is 110° because the widest $|S_{11}|$ and AR bandwidths are simultaneously achieved.

The $|S_{11}|$ and AR variations with dr are depicted in Figs. 16(a) and (b), respectively. Due to the small electrical size of dr, its variation has little effect on the impedance of the antenna, as shown in Fig. 16(a). However, the variation of dr affects the phase difference between the two orthogonal field components and therefore affects the CP radiation behavior and the AR bandwidth. When dr increases from 0.5mm to 2.5mm, the lower side frequency of 3 dB AR increases, and the upper side frequency decreases, so the 3 dB AR bandwidth decreases, as shown in Fig. 16(b). For a compromise, the value of dr is chosen to be 0.5 mm.

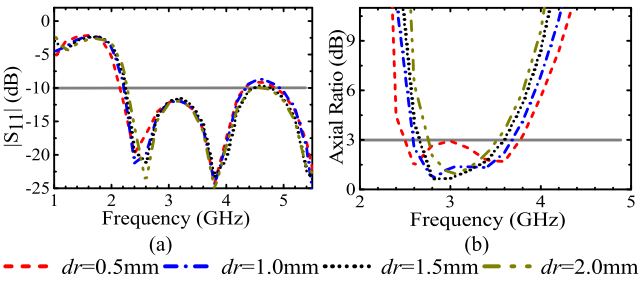

FIGURE 16. (a) Simulated $|S_{11}|$, and (b) AR of the proposed antenna with different *dr*.

The final values of each parameter are $R = 14$mm, $dr = 0.5$mm, $Py = 19$mm, $\alpha = 110°$, $Gx = 8$mm, and $Gy = 5$mm. The full-wave simulation indicates that the impedance band ($|S_{11}| < -10$ dB) and AR band (AR < 3 dB) of the proposed antenna are 68.7% (2.1 GHz–4.3 GHz) and 42.6% (2.4 GHz–3.7 GHz), respectively.

IV. EXPERIMENTAL VERIFICATION

As shown in Fig. 17, a prototype of the proposed antenna was fabricated and measured to verify the design procedure. The proposed antenna is fabricated by PCB technology. Multiple-amplitude-component method and comparison method are employed to measure AR and boresight gain, respectively. The KEYSIGHT N5222A vector network analyzer (VNA) is used to measure S-parameter. The VNA was calibrated by the short-open-load-through calibration before measurement. The distance between the antennas inside the anechoic chamber during the measurements is about 8 meters, which satisfies the far-field conditions of the proposed antenna and the standard antennas. The simulated and measured $|S_{11}|$, AR, and the boresight gain are all presented in Fig. 18. As can be seen, the measured −10 dB impedance bandwidth is 84.6% (2.35 GHz–5.8 GHz), and the measured 3 dB AR bandwidth is 43.4% (2.4 GHz–3.73 GHz). The overlapping operating band covers ISM band (2.4 GHz–2.483 GHz), TD-LTE band (2.599 GHz–2.690 GHz), and WiMAX bands (2.496 GHz–2.69 GHz and 3.4 GHz–3.6 GHz). The measured $|S_{11}|$ agrees well with the simulated $|S_{11}|$, and the slight difference is mainly due to the dimensional tolerance and undesired slot introduced by welding. The discrepancies between the measured and the simulated 3 dB AR bandwidth are probably caused by many reasons, such as the fabrication tolerance as well as the alignment problems in the measurement setup.

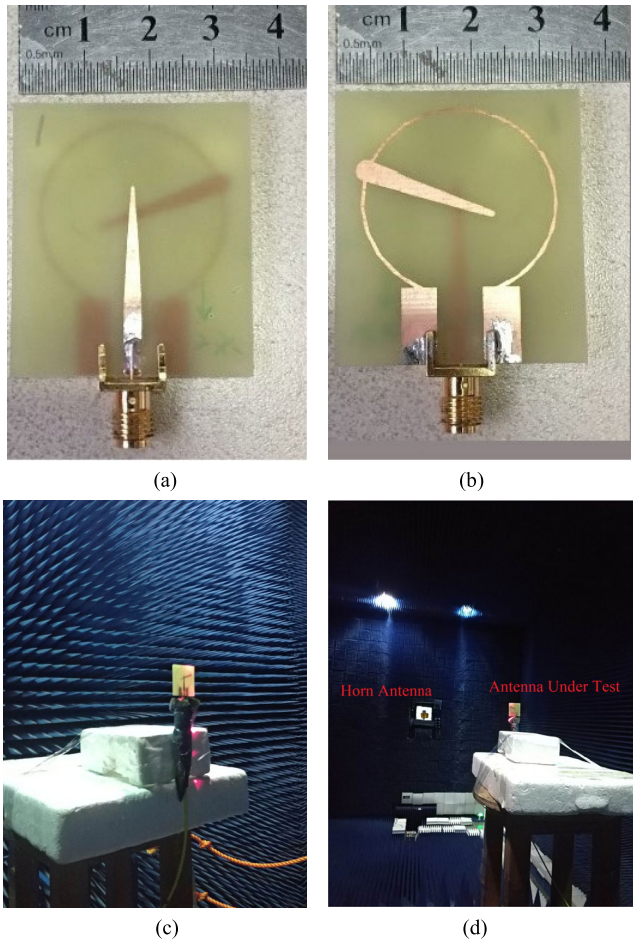

(a) (b) (c) (d)

FIGURE 17. (a) The top view of the proposed antenna. (b) The back view of the proposed antenna. (c) The proposed antenna under test. (d) Far-field measurement environment in the chamber.

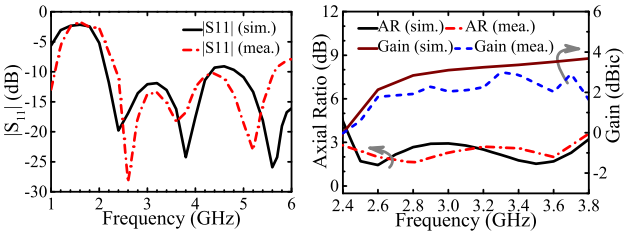

(a) (b)

FIGURE 18. Simulated and measured (a) $|S_{11}|$, (b) AR and boresight gain.

The simulated and measured radiation patterns in the XOY and YOZ planes at 2.4 GHz, 3.1 GHz, and 3.7 GHz are respectively plotted in Fig. 19. Bidirectional radiation patterns can be observed featuring the left-handed circularly polarized (LHCP) in the +Z direction and right-handed circularly polarized (RHCP) in the −Z direction. The comparisons with other works are listed in Table 1. In [26], smaller electrical size is obtained by using a stacked technology for the antenna, but the AR bandwidth is much lower than that of the proposed. In [27], the AR bandwidth of the antenna reaches 47.9%, but the profile is $0.15\lambda_L$, and the multi-feed structure increases fabrication complexity. In [28], [29], [30], [31], antennas suffer narrower AR bandwidth.

TABLE 1. Comparison between different circularly polarized antennas.

Ref.	AR<3 dB BW[a] &CF[b]	$\|S_{11}\|$<10 dB BW & CF	Dimensions ($\lambda_L \times \lambda_L \times \lambda_L$[c])
[26]	11.5%, 4.89 GHz	27.7%, 4.70 GHz	0.26×0.23×0.025
[27]	47.9%, 1.78 GHz	54.75%, 1.79GHz	0.53×0.53×0.15
[28]	16.6%, 4.53 GHz	25.3%, 4.14 GHz	0.38×0.38×0.20
[29]	34.8%, 1.83 GHz	53.0%, 2.00 GHz	0.18×0.18×0.088
[30]	20.4%, 6.00 GHz	48.6%, 5.96 GHz	0.80×0.78×0.096
[31]	23.0%, 3.23 GHz	41.0%, 3.13 GHz	0.39×0.32×0.017
[32]	96.6%, 7.16GHz	140.6%, 6.43GHz	0.74×0.49×0.012
[33]	91%, 3.85GHz	55%, 4.5GHz	0.29×0.29×0.01
[34]	95.7%, 2.3GHz	132%, 2.5GHz	0.24×0.16×0.004
[35]	129%, 3.89GHz	129%, 3.89GHz	0.19×0.19×0.006
This work	43.4%, 3.07 GHz	84.6%, 4.00 GHz	0.28×0.22×0.013

[a]BW: bandwidth.
[b]CF: center frequency.
[c]λ_L: Maximum wavelength of 3 dB AR band.

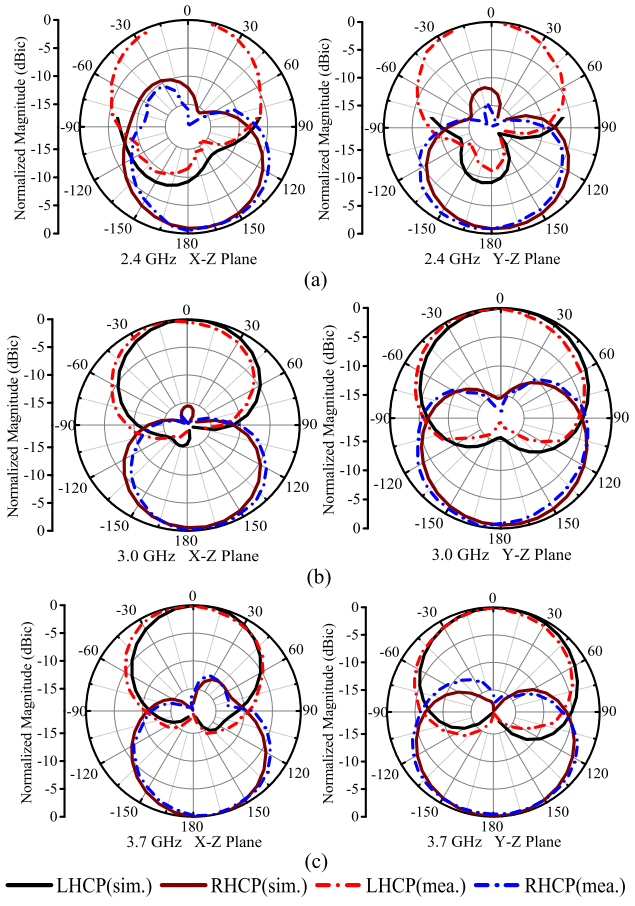

FIGURE 19. Simulated and measured normalized radiation patterns at (a) 2.4 GHz, (b) 3 GHz, and (c) 3.7 GHz.

In [32], [33], [34], [35], those bidirectional antennas achieve larger AR bandwidth than the proposed antenna, but the proposed antenna is superior to them in terms of radiation pattern stability. Considering the dimension, impedance bandwidth, AR bandwidth, and process complexity, the performance of the proposed antenna has certain advantages.

V. CONCLUSION

The clock-shaped circularly polarized antenna has been proposed based on characteristic mode analysis. To achieved CP operation, two microstrip lines have been introduced for the original circular ring, where three characteristic modes have been selected and combined accordingly. The feed-free structure satisfied the AR characteristics and operating bandwidth. With the guideline of CMA, the feed structure has been set at the appropriate position and excited the desired modes. The full-wave optimization has been carried out for wideband AR, impedance matching, and radiation performance. The measured results have demonstrated the proposed antenna. The design method of the CP antenna can be extended to other types of structures with clear theoretical explanations and directional guidance for optimization.

REFERENCES

[1] S.-L. S. Yang, A. A. Kishk, and K.-F. Lee, "Wideband circularly polarized antenna with L-shaped slot," *IEEE Trans. Antennas Propag.*, vol. 56, no. 6, pp. 1780–1783, Jun. 2008.
[2] C.-J. Wang and W.-B. Tsai, "Microstrip open-slot antenna with broadband circular polarization and impedance bandwidth," *IEEE Trans. Antennas Propag.*, vol. 64, no. 9, pp. 4095–4098, Sep. 2016.
[3] G. Yang, M. Ali, and R. Dougal, "A wideband circularly polarized microstrip patch antenna for 5–6-GHz wireless LAN applications," *Microw. Opt. Technol. Lett.*, vol. 45, no. 4, pp. 279–285, May 2005.
[4] S. Dentri, C. Phongcharoenpanich, and K. Kaemarungsi, "Single-fed broadband circularly polarized unidirectional antenna using folded plate with parasitic patch for universal UHF RFID readers," *Int. J. RF Microw. Comput.-Aided Eng.*, vol. 26, no. 7, pp. 575–587, Sep. 2016.
[5] T. N. Chang, "Circularly polarized antenna for 2.3–2.7 GHz WiMax band," *Microw. Opt. Technol. Lett.*, vol. 51, no. 12, pp. 2921–2923, Dec. 2009.
[6] J. Y. Sze, J. C. Wang, and C. C. Chang, "Axial-ratio bandwidth enhancement of asymmetric-CPW-fed circularly-polarised square slot antenna," *Electron. Lett.*, vol. 44, no. 18, pp. 1048–1049, Aug. 2008.
[7] J.-Y. Sze and S.-P. Pan, "Design of CPW-fed circularly polarized slot antenna with a miniature configuration," *IEEE Antennas Wireless Propag. Lett.*, vol. 10, pp. 1465–1468, 2011.
[8] S. H. Yeung, K. F. Man, and W. S. Chan, "A bandwidth improved circular polarized slot antenna using a slot composed of multiple circular sectors," *IEEE Trans. Antennas Propag.*, vol. 59, no. 8, pp. 3065–3070, Aug. 2011.
[9] J. Y. Jan, C. Y. Pan, K. Y. Chiu, and H. M. Chen, "Broadband CPW-fed circularly-polarized slot antenna with an open slot," *IEEE Trans. Antennas Propag.*, vol. 61, no. 3, pp. 1418–1422, Mar. 2013.
[10] T.-N. Chang, "Wideband circularly polarised antenna using two linked annular slots," *Electron. Lett.*, vol. 47, no. 13, pp. 737–739, Jun. 2011.
[11] S. Fu, S. Fang, Z. Wang, and X. Li, "Broadband circularly polarized slot antenna array fed by asymmetric CPW for L-band applications," *IEEE Antennas Wireless Propag. Lett.*, vol. 8, pp. 1014–1016, 2009.
[12] J. Pourahmadazar and V. Rafii, "Broadband circularly polarised slot antenna array for L- and S-band applications," *Electron. Lett.*, vol. 48, no. 10, pp. 542–543, May 2012.
[13] R. J. Garbacz and R. Turpin, "A generalized expansion for radiated and scattered fields," *IEEE Trans. Antennas Propag.*, vol. 19, no. 3, pp. 348–358, May 1971.
[14] R. F. Harrington and J. R. Mautz, "Theory of characteristic modes for conducting bodies," *IEEE Trans. Antennas Propag.*, vol. AP-19, no. 5, pp. 622–628, Sep. 1971.
[15] Y. K. Chen and C.-F. Wang, *Characteristic Modes: Theory and Applications in Antenna Engineering*. Hoboken, NJ, USA: Wiley, 2015, pp. 52–55.
[16] F. H. Lin and Z. N. Chen, "Probe-fed broadband low-profile metasurface antennas using characteristic mode analysis," in *Proc. IEEE 6th Asia–Pacific Conf. Antennas Propag. (APCAP)*, Xi'an, China, Oct. 2017, pp. 1–3.
[17] F. H. Lin, Z. N. Chen, W. Liu, and Z. N. Chen, "A metamaterial-based broadband circularly polarized aperture-fed grid-slotted patch antenna," in *Proc. IEEE 4th Asia–Pacific Conf. Antennas Propag. (APCAP)*, Kuta, Indonesia, Jun./Jul. 2015, pp. 353–354.
[18] F. H. Lin and Z. N. Chen, "Low-profile wideband metasurface antennas using characteristic mode analysis," *IEEE Trans. Antennas Propag.*, vol. 65, no. 4, pp. 1706–1713, Apr. 2017.
[19] F. H. Lin and Z. N. Chen, "A method of suppressing higher order modes for improving radiation performance of metasurface multiport antennas using characteristic mode analysis," *IEEE Trans. Antennas Propag.*, vol. 66, no. 4, pp. 1894–1902, Apr. 2018.
[20] T. Li and Z. N. Chen, "A dual-band metasurface antenna using characteristic mode analysis," *IEEE Trans. Antennas Propag.*, vol. 66, no. 10, pp. 5620–5624, Oct. 2018.
[21] T. Li and Z. N. Chen, "Metasurface-based shared-aperture 5G *S-/K*-band antenna using characteristic mode analysis," *IEEE Trans. Antennas Propag.*, vol. 66, no. 12, pp. 6742–6750, Dec. 2018.
[22] T. Li and Z. N. Chen, "Wideband substrate-integrated waveguide-fed end-fire metasurface antenna array," *IEEE Trans. Antennas Propag.*, vol. 66, no. 12, pp. 7032–7040, Dec. 2018.
[23] L. Minz, R. S. Aziz, M. T. Azim, and S. O. Park, "Wideband aperture-coupled stack-patch antenna design with characteristic mode analysis," in *Proc. IEEE Int. Conf. Consum. Electron.-Asia (ICCE-Asia)*, Jeju, South Korea, Jun. 2018, pp. 206–212.

[24] A. Sharif, J. Ouyang, F. Yang, H. T. Chattha, M. A. Imran, A. Alomainy, and Q. H. Abbasi, "Low-cost, inkjet-printed UHF RFID tag based system for Internet of Things applications using characteristic modes," *IEEE Internet Things J.*, vol. 6, no. 2, pp. 3962–3975, Apr. 2019.
[25] M. Khan and D. Chatterjee, "Characteristic mode analysis of a class of empirical design techniques for probe-fed, U-slot microstrip patch antennas," *IEEE Trans. Antennas Propag.*, vol. 64, no. 7, pp. 2758–2770, Jul. 2016.
[26] S. Shekhawat, P. Sekra, D. Bhatnagar, V. K. Saxena, and J. S. Saini, "Stacked arrangement of rectangular microstrip patches for circularly polarized broadband performance," *IEEE Antennas Wireless Propag. Lett.*, vol. 9, pp. 910–913, 2010.
[27] C. Lin, F.-S. Zhang, Y.-C. Jiao, F. Zhang, and X. Xue, "A three-fed microstrip antenna for wideband circular polarization," *IEEE Antennas Wireless Propag. Lett.*, vol. 9, pp. 359–362, 2010.
[28] S. S. Yang, K.-F. Lee, and A. A. Kishk, "Design and study of wideband single feed circularly polarized microstrip antennas," *Prog. Electromagn. Res.*, vol. 80, pp. 45–61, 2008.
[29] K.-L. Wong and T.-W. Chiou, "Single-patch broadband circularly polarized microstrip antennas," in *Proc. IEEE Antennas Propag. Soc. Int. Symp.*, Salt Lake City, UT, USA, Jul. 2000, pp. 984–987.
[30] T. Nakamura and T. Fukusako, "Broadband design of circularly polarized microstrip patch antenna using artificial ground structure with rectangular unit cells," *IEEE Trans. Antennas Propag.*, vol. 59, no. 6, pp. 2103–2110, Jun. 2011.
[31] X. L. Bao, M. J. Ammann, and P. McEvoy, "Microstrip-fed wideband circularly polarized printed antenna," *IEEE Trans. Antennas Propag.*, vol. 58, no. 10, pp. 3150–3156, Oct. 2010.
[32] R. Xu, J. Y. Li, K. Wei, and G. W. Yang, "Broadband rotational symmetry circularly polarised antenna," *Electron. Lett.*, vol. 52, no. 6, pp. 414–416, Mar. 2016.
[33] H. H. Tran, N. Nguyen-Trong, and A. M. Abbosh, "Simple design procedure of a broadband circularly polarized slot monopole antenna assisted by characteristic mode analysis," *IEEE Access*, vol. 6, pp. 78386–78393, 2018.
[34] R. Xu, J.-Y. Li, and J. Liu, "A design of broadband circularly polarized C-shaped slot antenna with sword-shaped radiator and its array for L/S-band applications," *IEEE Access*, vol. 6, pp. 5891–5896, 2018.
[35] D. S. Chandu and S. S. Karthikeyan, "Broadband circularly polarized printed monopole antenna with protruded L-shaped and inverted L-shaped strips," *Microw. Opt. Technol. Lett.*, vol. 60, pp. 242–248, Jan. 2018.

MIN HAN received the B.S. degree in electronic information engineering from Qufu Normal University, Qufu, China, in 2010, and the M.S. degree in information and communication engineering from the Nanjing University of Science and Technology, Nanjing, China, in 2013. She is currently pursuing the Ph.D. degree in electromagnetic field and microwave engineering with Southeast University, Nanjing, China. Her current research interests include broadband circularly polarized antennas and direction of arrival. She received the awards and honors include the Best student paper Award of UCMMT 2012 and the Ph.D. Scholarship of Rod and Schwartz 2018.

WENBIN DOU (M'94–SM'12) received the B.S degree from the University of Science and Technology of China, Hefei, China, in 1978, and the M.S. and Ph.D. degrees from the University of Electronic Science and Technology of China, Chengdu, China, in 1983 and 1987, respectively. Since 1994, he has been a Professor with Southeast University, Nanjing, China, where he serves as the Vice Director for the State Key Laboratory of Millimeter Waves. His current research interests include ferrite devices, quasi-optics, millimeter-wave focal imaging, antennas and scattering, and millimeter-wave binary optics. He is also a Fellow of the Chinese Institute of Electronics (CIE) and a Committee Member of the Microwave Institute, CIE. He is also the Co-Chairman of the Program Committee of IRMMW-THz.